

Electric field control and effect of Pd capping on magnetocrystalline anisotropy in FePd thin films: A first-principles study

P. V. Ong,¹ Nicholas Kioussis,^{1,*} P. Khalili Amiri,² J. G. Alzate,² K. L. Wang,² Gregory P. Carman,³ Jun Hu,⁴ and Ruqian Wu⁴

¹*Department of Physics and Astronomy, California State University Northridge, Northridge, California 91330, USA*

²*Department of Electrical Engineering, University of California, Los Angeles, California 90095, USA*

³*Department of Mechanical and Aerospace Engineering, University of California, Los Angeles, California 90095, USA*

⁴*Department of Physics and Astronomy, University of California, Irvine, California 92697-4575, USA*

(Received 10 January 2014; revised manuscript received 8 March 2014; published 24 March 2014)

Using *ab initio* electronic structure calculations, we have investigated the effect of an electric field and of a heavy-metal cap of Pd on the magnetocrystalline anisotropy (MCA) of FePd ultrathin film. Analysis of the energy- and k -resolved distribution of the orbital character of the minority-spin band reveals that the perpendicular MCA of the uncapped film mainly arises from the spin-orbit coupling (SOC) between unoccupied Fe d_{xy} and occupied Fe $d_{x^2-y^2}$ states. On the other hand, the SOC between the Pd- and Fe-derived d states yields negative contributions to the MCA. We find that the sensitivity of the surface anisotropy energy to the applied electric field is 18 fJ/(Vm) and is due to changes in the occupation of the surface Fe atoms $d_{x^2-y^2}$ and (d_{xz}, d_{yz}) orbitals. We demonstrate that the thickness of the Pd cap has a dramatic effect on the MCA and can even switch the magnetization from out-of- to in-plane orientation. The underlying origin is the change of the position and orbital character of the spin-polarized quantum well states induced in the Pd cap by varying its thickness. These results have important implications for exploiting heavy metals with large spin-orbit coupling (Ru, Pd, Ta, Pt, or Au) as contacts with ferromagnetic thin films to tailor the magnetic switching of spintronic devices by tuning the cap thickness.

DOI: [10.1103/PhysRevB.89.094422](https://doi.org/10.1103/PhysRevB.89.094422)

PACS number(s): 75.30.Gw, 75.70.Cn, 75.85.+t, 73.20.-r

I. INTRODUCTION

Spin-current-induced torque in a magnetic tunnel junction offers a potential for the realization of low-power and highly scalable random access memory (RAM), compared with the conventional magnetoresistive RAM, in which magnetization reversal is induced by the magnetic field [1,2]. However, this approach requires a high critical current density for magnetization switching, leading to immense Ohmic dissipation and high-power consumption [2]. For low-power spintronic devices, one promising approach is to control the magnetocrystalline anisotropy (MCA) of a thin ferromagnetic film (FM) by an external electric field (E-field). Important progress towards this direction was made when it was demonstrated that the MCA of L1₀-ordered FePt and FePd ultrathin films immersed in an electrolyte can be modified by applying an E-field [3]. Recently, the E-field-induced modification of MCA has been reported for magnetic monolayers [4], surfaces of Fe [5] or Fe/Pt multilayers [6,7], and Fe/MgO or FeCoB/MgO interfaces [8–11]. Moreover, a voltage-assisted magnetization switching has been realized in Au/Fe_{0.8}Co_{0.2}/MgO [12].

The MCA depends sensitively on the details of the electronic states near the Fermi level. The contribution of the spin-orbit coupling (SOC) between electronic states to the MCA strongly varies over the Brillouin zone [13]. Although there is a general consensus that the modification of the MCA stems from changes in the relative occupation of transition-metal d orbitals [3,8], the mechanism of the E-field-induced MCA is not well understood, such as the sign reversal of the voltage dependence of the MCA in FePd and FePt thin films [3,14]. Different dependencies of the voltage-induced

MCA have also been observed in CoFeB/MgO junctions when different capping materials of heavy metals (Ru, Pd, Ta, Pt, Au) are employed as the contact electrode [15]. This raises an intriguing question regarding the influence of overlayers on the MCA at the FM/heavy-metal interfaces. It has also been shown that a Pd overlayer of 11 monolayers (ML) on an FePd film may induce the formation of a new phase near the FePd/Pd interface that exhibits in-plane MCA and strongly modifies the effective MCA of the whole thin film [16]. Another experiment on Fe_{0.5}Pd_{0.5}/MgO ultrathin films showed that Pd capping causes an in-plane to out-of-plane magnetic easy axis transition for an FePd film with thickness around 9 ML, and reported high E-field sensitivity of the effective MCA of about 600 fJ/(Vm) [17].

The objective of this work is to carry out first-principles electronic structure calculations to study the MCA of FePd films and the effect of Pd capping. The rest of this paper is organized as follows: Section II describes the methodology used to calculate the MCA. In Sec. III A, we discuss the origin of perpendicular MCA in thin FePd films. In Sec. III B, we elucidate the mechanism of the E-field control of MCA by analyzing the E-field-induced redistribution of the transition-metal d orbitals. In Sec. III C, we demonstrate that the heavy-metal capping has a strong effect on the MCA of the whole film and that the magnetization can be switched from perpendicular to in-plane MCA by tuning the capping thickness. Finally, conclusions are summarized in Sec. IV.

II. COMPUTATIONAL METHODS AND MODELS

Thin films of FePd(001) with Fe termination are modeled by slab supercells with a surface area of $a/\sqrt{2} \times a/\sqrt{2}$, where a is the equilibrium lattice constant of the bulk L1₀ ordered

*nick.kioussis@csun.edu

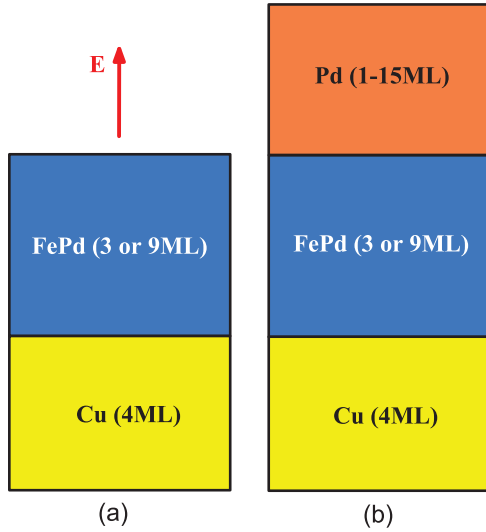


FIG. 1. (Color online) Schematic models for the calculation of the MCA of FePd thin films (a) with and (b) without Pd capping. The arrow indicates the positive direction of the E-field.

FePd. The vacuum region of the supercells is fixed at 15\AA . In order to investigate the E-field dependence of the MCA of the FePd film, a 4-ML-thick nonmagnetic layer of Cu is used to cover one of the film surfaces [Fig. 1(a)]. The thickness of the Pd cap is varied in the range of 1–15 ML [Fig. 1(b)]. The FePd/Cu interface MCA, which is E-field independent, is calculated from a superlattice model and then subtracted from that of the whole slab.

First-principles density functional calculations are performed within the framework of the plane-wave projector augmented wave formalism [18], as implemented in the Vienna *ab initio* simulation package (VASP) code [19–21]. The generalized gradient approximation (GGA) is employed to treat the exchange-correlation interaction. Ionic and electronic degrees of freedom are relaxed simultaneously at the zero field until the forces acting on the ions become less than $0.3 \times 10^{-3} \text{ eV/\AA}$ and the change in the total energy between two ionic relaxation steps is smaller than 10^{-6} eV . The resulting atomic structures are then used for calculations with an applied E-field. The plane-wave cutoff energy is 500 eV and the Monkhorst-Pack k mesh is $15 \times 15 \times 1$ ($31 \times 31 \times 1$) for the relaxations (relativistic calculations). The dipole correction [22] to the total energy is applied. The valence electrons are treated in the scalar relativistic approximation. The SOC of the valence electrons is then included using the second-variation method [23] employing the scalar-relativistic eigenfunctions of the valence states. The MCA was calculated as the total-energy difference between two magnetic states in which the magnetization is aligned along the [100] or [001] directions, respectively, i.e., $\text{MCA} = E[100] - E[001]$.

III. RESULTS AND DISCUSSION

A. Origin of perpendicular MCA

Figure 2(a) displays the variation of the magnetic moment of the surface Fe atom in the 9 ML FePd (001) film under

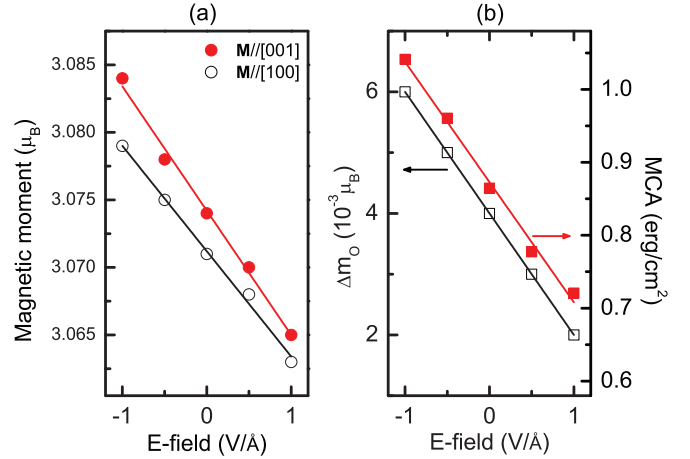


FIG. 2. (Color online) (a) Total magnetic moment on the surface Fe in the 9-ML-thick FePd film vs the E-field, with the moment along the [100] and [001] direction, respectively. (b) Difference in orbital moment of the surface Fe between the [001] and [100] orientation (left scale) and the MCA of the thin film (right scale) as a function of the E-field.

the influence of the E-field for magnetization lying either in the plane of the film ([100] direction) or perpendicular to the plane ([001] direction). Here, the positive E-field, shown in Fig. 1, corresponds to depletion of electrons from the FePd surface. In contrast to the freestanding Fe(001) film [5], the magnetic moment of Fe in the FePd film decreases linearly with positive field. It is well known that in the FePd multilayer, the Fe 3d-Pd 4d hybridization induces significant shifts in the energy bands and changes the occupations of Fe 3d states near the Fermi level. For the freestanding Fe(001) surface or the Fe/MgO(001) interface, the density of states (DOS) around the Fermi energy arises mainly from the minority-spin $t_{2g}(d_{xz}, d_{yz})$ states [24–26]. On the other hand, for the FePd film, the surface minority-spin DOS at the Fermi level has dominant $e_g(d_{x^2-y^2})$ orbital character. The majority-spin bands in both cases are almost fully occupied and are well below E_F . The E-field-induced surface magnetic moment is given by $\mu_0 \Delta M = \alpha_S E$ (SI units), where μ_0 is the vacuum magnetic permeability and α_S is the surface magnetoelectric coefficient. We find that $\alpha^{100} = 1.2 \times 10^{-14} \text{ G cm}^2/\text{V}$ and $\alpha^{001} = 1.4 \times 10^{-14} \text{ G cm}^2/\text{V}$, for the in-plane and out-of-plane magnetization, respectively.

Figure 2(b) shows the difference between the out-of- and in-plane orbital moments for the surface Fe, i.e., $\Delta m_o = m_o^{[001]} - m_o^{[100]}$, and the MCA of the thin film as a function of the E-field. The results show that the Bruno expression [27], $\text{MCA} = \xi \Delta m_o / (4\mu_B)$, where ξ is the SOC constant, is satisfied. The value of ξ averaged over the applied E-field is 48 meV. We find that the sensitivity of MCA to the E-field [the slope of MCA in Fig. 2(b)] is about 18 fJ/(Vm) compared to the corresponding values of 33 and 26 fJ/(Vm) for a monolayer Fe(001) [24] and a 15-ML-thick Fe(001) [5], respectively.

In order to elucidate the origin of the perpendicular MCA of the FePd film, we show in Fig. 3 the k -resolved MCA along the high-symmetry directions in the two-dimensional Brillouin zone. According to the force theorem, this quantity can be

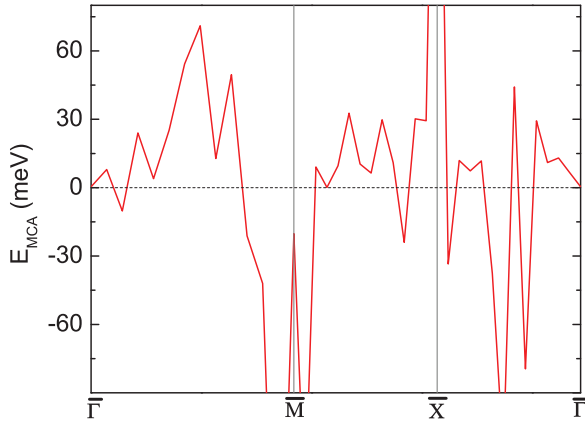


FIG. 3. (Color online) The k -resolved MCA along the high-symmetry directions in the two-dimensional Brillouin zone.

expressed approximately as $\text{MCA}(\mathbf{k}) \approx \sum_{n \in \text{occ}} [\varepsilon(n, \mathbf{k})^{[100]} - \varepsilon(n, \mathbf{k})^{[001]}]$, where $\varepsilon(n, \mathbf{k})^{[100]}$ and $\varepsilon(n, \mathbf{k})^{[001]}$ are the eigenvalues of the Hamiltonian for magnetization along the [100] and [001] direction, respectively, and the band index n runs over the occupied bands [28,29]. Overall, the sum of the MCA(\mathbf{k}) over k points yields a positive (perpendicular) MCA. In particular, the MCA(\mathbf{k}) exhibits two main positive peaks around $\frac{1}{2}(\bar{\Gamma} - \bar{M})$ and \bar{X} , and two main negative peaks around \bar{M} and $\frac{1}{2}(\bar{\Gamma} - \bar{X})$. Within the second-order perturbation of the total energy due to the SOC, the MCA is not only determined by the orbital character of the occupied states, but it also depends on the couplings between the occupied and empty states through the orbital angular momentum operators \hat{L}_x and \hat{L}_z and on the energy difference between these states. Namely, the MCA can be expressed as [13]

$$\text{MCA} \propto \xi^2 \sum_{o,u} \frac{|\langle \Psi_o^\downarrow | \hat{L}_z | \Psi_u^\downarrow \rangle|^2 - |\langle \Psi_o^\downarrow | \hat{L}_x | \Psi_u^\downarrow \rangle|^2}{E_u^\downarrow - E_o^\downarrow}, \quad (1)$$

where Ψ_o^\downarrow and Ψ_u^\downarrow indicate the occupied and unoccupied minority-spin bands. Note that the corresponding contribution to the MCA from the majority-spin bands is small due to the fact that the majority-spin states are well below the Fermi energy. Furthermore, the MCA contribution from the SOC between states of opposite spin has been shown to be small [13].

In transition-metal systems, the positive contribution to the MCA originates from two matrix elements of $\langle x^2 - y^2 | \hat{L}_z | xy \rangle$ and $\langle xz | \hat{L}_z | yz \rangle$, i.e., coupling between the d_{xy} and $d_{x^2-y^2}$ orbitals and between the d_{xz} and d_{yz} orbitals through the \hat{L}_z operator. Detailed analysis of the band structure reveals that the $d_{x^2-y^2}$ orbital is the dominant character of the occupied states near the Fermi energy, while the d_{xy} , d_{xz} , d_{yz} , and $d_{3z^2-r^2}$ derived orbitals lie mainly above the Fermi energy. In Fig. 4, we show the energy- and k -resolved distribution of the Fe-derived d_{xy} and $d_{x^2-y^2}$ orbital character, respectively, where the color denotes the orbital character of the specific d orbital. One can clearly see that the unoccupied (occupied) Fe states along most of the $(\bar{\Gamma} - \bar{M})$ and $(\bar{\Gamma} - \bar{X})$ symmetry directions are primarily of d_{xy} ($d_{x^2-y^2}$) orbital character. Furthermore, the energy difference between these states decreases around the

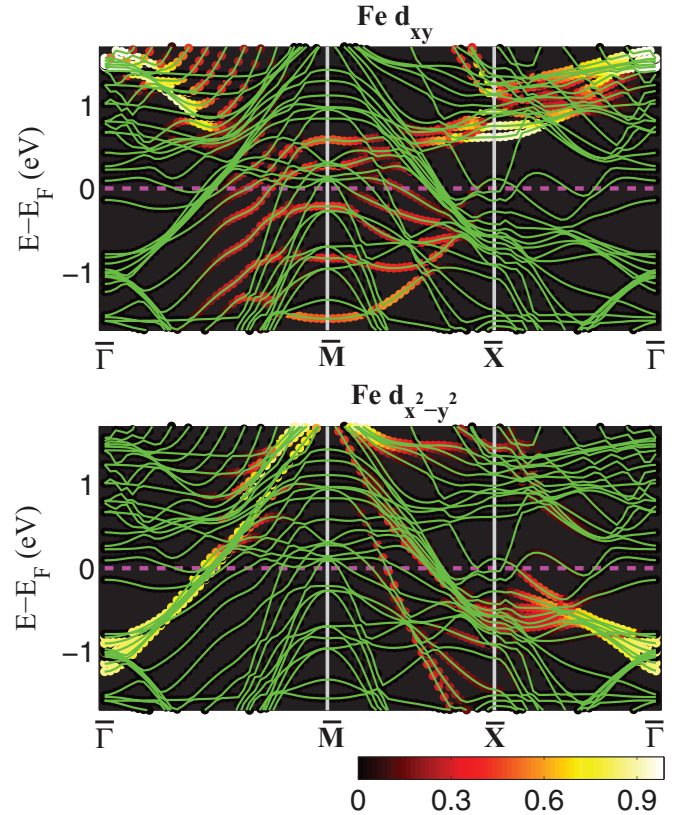


FIG. 4. (Color online) Energy- and k -resolved distribution of the orbital character of the minority-spin band of the 9 ML FePd film for the Fe d_{xy} (upper panel) and $d_{x^2-y^2}$ (lower panel) states. The color denotes the amplitude of the d -orbital character. The horizontal line denotes the Fermi level.

$\frac{1}{2}(\bar{\Gamma} - \bar{M})$ and at \bar{X} , leading to the main positive peaks of the k -resolved MCA.

The diagram of the energy levels for the minority-spin band at the $\bar{\Gamma}$ and \bar{M} points is shown in Fig. 5. The red (blue) horizontal lines denote the Fe- (Pd)-derived bands and the green line denotes Fe- d_{z^2} /Pd- d_{z^2} hybridized bands, where the thickness of the lines is proportional to the specific d -orbital character. The SOC of this hybridized state to the unoccupied Fe-derived (d_{xz} , d_{yz}) and d_{xy} states gives a negative contribution to the MCA. We find that the states close to the Fermi energy (both below and above) at the \bar{M} and $\bar{\Gamma}$ points are Pd-derived d_{z^2} and $d_{x^2-y^2}$ states. Note that the SOC of the Pd occupied d_{z^2} states with the Fe unoccupied (d_{xz} , d_{yz}) states and the occupied Fe (d_{xz} , d_{yz}) states with the Pd unoccupied $d_{x^2-y^2}$ states, as well as the SOC between the Fe d -derived states, yield negative contributions to the k -resolved MCA at \bar{M} .

B. Mechanism of electric field control of MCA

In order to elucidate the underlying mechanism of the E-field-induced change of the MCA in the FePd film, we show in Fig. 6 the change of the k -resolved MCA under an external E-field relative to its zero-field value, $\Delta \text{MCA}(\mathbf{k}) = \text{MCA}^E(\mathbf{k}) - \text{MCA}^0(\mathbf{k})$, for (a) -0.5 V/\AA and (b) 0.5 V/\AA , respectively. A comparison of Figs. 6(a) and 6(b) shows that the main change

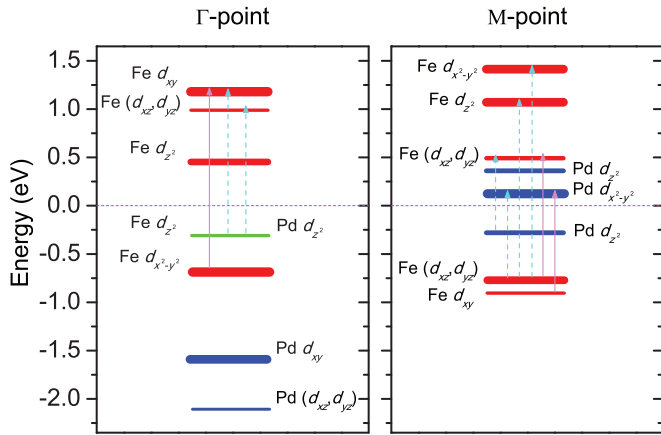


FIG. 5. (Color online) Energy-level diagram of the minority-spin states of the 9 ML FePd film at the $\bar{\Gamma}$ and \bar{M} points relative to the Fermi energy (horizontal dashed line). The red (blue) horizontal lines denote the Fe- (Pd)-derived bands and the green line denotes the Fe- d_{z^2} /Pd- d_{z^2} hybridized bands, where the thickness of the lines is proportional to the specific d -orbital character. The solid (dashed) vertical arrows indicate the SOC between various occupied and unoccupied states which give positive (negative) contribution to the MCA.

in $\Delta\text{MCA}(\mathbf{k})$ upon reversal of the E-field direction occurs primarily around the $\frac{1}{2}(\bar{\Gamma} - \bar{M})$, where the positive broad peak under -0.5 V/\AA changes to negative under 0.5 V/\AA . This results in an E-field-induced increase (decrease) of the MCA under negative (positive) E-field (Fig. 2), corresponding to accumulation (depletion) of electrons at the FePd surface. Due to the short Thomas-Fermi screening length in the metal, the effect of the external field is mainly localized at the surface layers. Thus, in Fig. 7, we display the energy- and k -resolved distribution of the surface Fe-derived d_{xy} and $d_{x^2-y^2}$ orbitals, respectively, where the color denotes the orbital character of

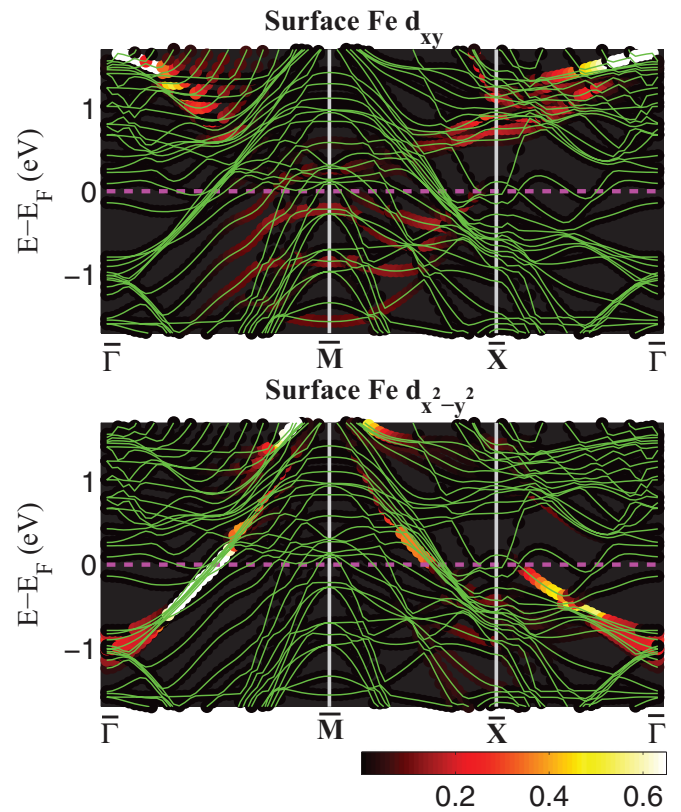


FIG. 7. (Color online) Energy- and k -resolved distribution of the orbital character of the minority-spin band of the 9 ML FePd film for the surface Fe d_{xy} (upper panel) and $d_{x^2-y^2}$ (lower panel), respectively. The color denotes the amplitude of the d -orbital character.

the specific d orbital. One can clearly see that the unoccupied (occupied) Fe surface states along $(\bar{\Gamma} - \bar{M})$ are primarily of d_{xy} ($d_{x^2-y^2}$) orbital character, indicating that the modification

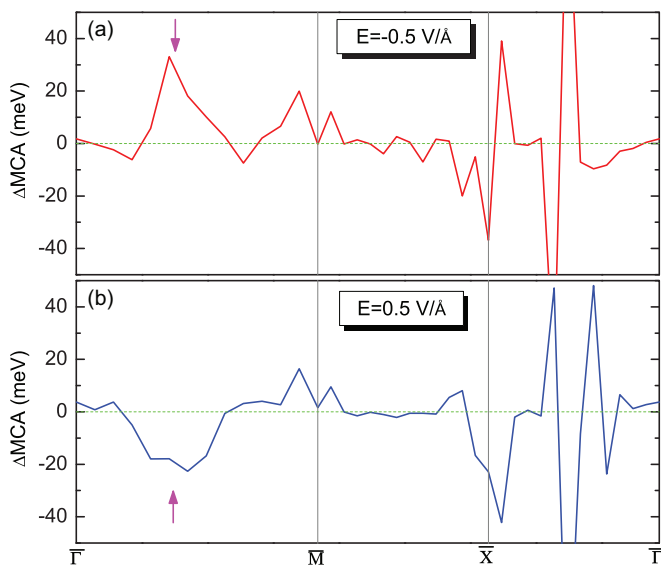


FIG. 6. (Color online) Difference in k -resolved MCA induced by the E-field of (a) -0.5 V/\AA and (b) 0.5 V/\AA relative to the zero-field case for the 9 ML FePd film. The arrows indicate the MCA peak that is strongly affected by the E-field reversal.

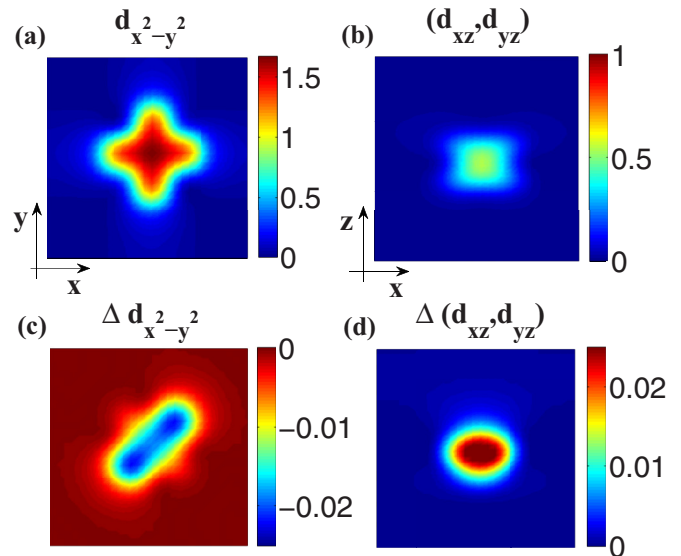


FIG. 8. (Color online) (a), (b) Surface charge densities of $d_{x^2-y^2}$ and (d_{xz}, d_{yz}) states, respectively, under zero field within an energy range of 0.6 eV below the Fermi level in the $\bar{\Gamma}\bar{M}$ region. (c), (d) Charge density differences induced by an E-field of 0.5 V/\AA . The unit of contour values is $e/\text{\AA}^3$.

of the SOC between these surface states is responsible for the E-field-induced change in MCA.

Figures 8(a) and 8(b) show the zero-field surface charge densities of the $d_{x^2-y^2}$ and (d_{xz}, d_{yz}) states, respectively, within the energy range of 0.6 eV below the Fermi level in the $\Gamma\bar{M}$ direction. The corresponding E-field-induced charge densities (i.e., difference in densities in the presence and absence of field) of these orbitals under an external field of 0.5 V/\AA are shown in Figs. 8(c) and 8(d), respectively. The positive (negative) values of the difference in charge densities of the d_{xz}, d_{yz} ($d_{x^2-y^2}$) orbitals indicates that the positive field induces a small $d_{x^2-y^2} \rightarrow (d_{xz}, d_{yz})$ charge transfer. Since the SOC of the occupied $d_{x^2-y^2}$ to unoccupied d_{xy} states is responsible for the main positive contribution to the MCA, the changes in the $d_{x^2-y^2}$ and (d_{xz}, d_{yz}) occupation result in the reduction of the MCA of the FePd film under a positive E-field. Our findings are consistent with experiment, which reported that an applied voltage of 200 V changes the electron filling by 2×10^{-3} electrons per Fe surface atom. However, such small changes of band filling can induce a large change in the MCA of the Fe/MgO(001) junction [8]. Therefore, the sign of the E-field dependence of the MCA is determined by the interplay of transition-metal surface d orbitals and the associated SOC present.

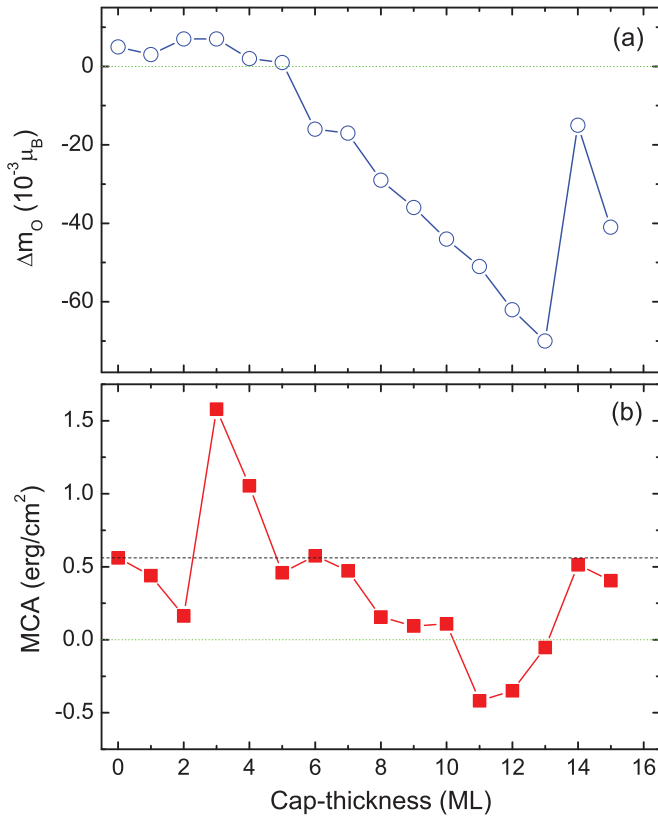


FIG. 9. (Color online) (a) Difference between the *total* orbital moment along the [001] and [100] directions and (b) the MCA of the 3-ML-FePd/*n*-ML-Pd system as a function of the Pd cap thickness. The horizontal dashed line in (b) denotes the MCA value of the uncapped FePd film.

C. Effect of Pd capping on magnetic anisotropy of FePd ultrathin film

In this section, we investigate the effect of the Pd capping on the MCA of a 3-ML-thick FePd film, where the Pd overlayer thickness was varied from 1 to 15 ML. As expected, the Pd cap becomes ferromagnetic due to the strong hybridization with the FePd thin film, giving rise to large changes of the MCA. In addition, the large interfacial relaxation plays an important role in the electronic and magnetic properties. We find that the magnetic moment of the interfacial Pd atoms is about $0.33\mu_B/\text{atom}$ and is independent of the Pd overlayer thickness. For $n < 14$ (n is the number of Pd overlayers), the magnetic moments of the whole Pd cap (including surface atoms) are $\sim 0.2\mu_B/\text{atom}$, indicating a long magnetic-moment decay length which in turn leads to the Pd-surface contribution to the effective MCA of the whole system. For larger thickness (above 13 Pd ML), the surface Pd atoms are practically nonmagnetic. The large long-range palladium polarization near the FePd/Pd interface arises both from the hybridization and the strain-induced volume expansion of about 5.4% (3.4%) at the FePd/Pd (Pd/vacuum) interface, in agreement with similar calculations on Fe/Pd (001) superlattices [30].

Figure 9(a) shows the variation of the difference between the *total* orbital moment of the 3-ML-FePd/*n*-ML-Pd slab along the [001] and [100] directions, $\Delta m_o = \sum_i (m_{o,i}^{[001]} - m_{o,i}^{[100]})$, as a function of the Pd cap thickness, where the site index i runs over all atoms in the system. Δm_o reaches a maximum at 3 ML and decreases monotonically with increasing Pd thickness, reaching its minimum value at 14 ML. The corresponding variation of the effective MCA of the 3-ML-FePd/*n*-ML-Pd slab with the Pd overlayer thickness

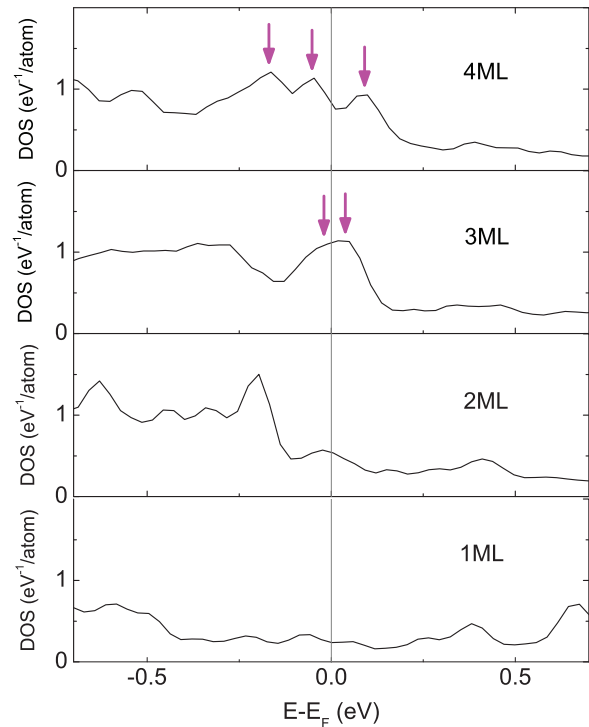


FIG. 10. (Color online) Total Pd d -derived DOS projected on and averaged over all MLs in the Pd cap for different Pd cap thickness. The arrows indicate the spin-polarized QWS near the Fermi level.

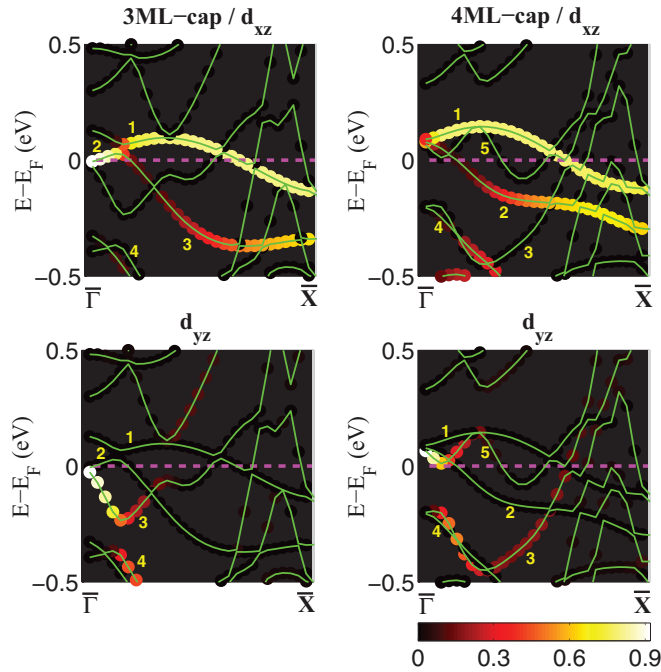


FIG. 11. (Color online) Energy- and k -resolved distribution of the Pd-cap-derived d_{xz} (top panel) and d_{yz} (bottom panel) orbitals of the minority-spin band along $\overline{\Gamma X}$ for the 3 ML FePd film capped with 3 ML (left panels) and 4 ML (right panels) of Pd, respectively. The various bands near the Fermi level are labeled by numbers.

[Fig. 9(b)] exhibits an oscillatory behavior and changes dramatically with the number of Pd ML. At 3 ML, the MCA has increased by a factor of three compared to its value of the uncapped FePd film (denoted by the horizontal dashed line); it

reverses sign at ~ 11 ML, favoring an in-plane magnetization alignment, and becomes positive again at 14 ML. Note that the variation of the MCA with n correlates with the corresponding variation of Δm_o shown in Fig. 9(a). It is worth mentioning that our calculations for the 9-ML-thick FePd film exhibit a similar oscillatory behavior as a function of Pd thickness, indicating that the capping effect is robust and its origin lies on the change of the electronic structure of the Pd cap upon varying its thickness, which is discussed below. The oscillation of the MCA versus Pd cap thickness is consistent with that found in thin Co films, where the uniaxial magnetic anisotropy oscillates as a function of film thickness with a period of about 2.3 atomic layers [31–34].

Figure 10 shows the total Pd d -derived DOS projected on and averaged over all MLs in the Pd cap. For the 1-ML-thick Pd cap, since the Pd overlayer is simply a continuation of the Fe-Pd stacking of the $L1_0$ -ordered structure, its electronic structure is similar to that of the Pd interior layer. The addition of a second Pd overlayer gives rise to a broad peak around the Fermi energy. As the Pd cap thickness increases, there is a series of occupied and unoccupied spin-polarized quantum well states (SPQWS) (denoted by vertical arrows) due to the electron confinement normal to the slab. The number and energy levels of the SPQWS depend on the thickness of the Pd cap. Note that the small energy separation between the occupied and unoccupied states close to the Fermi energy for the 3 ML cap is responsible for the large enhancement of the MCA in Fig. 9(b).

In order to elucidate the orbital character of the pertinent SPQWS in the Pd cap, we display in Fig. 11 the energy- and k -resolved distribution of the the Pd-cap-derived d_{xz} and d_{yz} orbitals along the $\overline{\Gamma X}$ direction for the 3 ML and 4 ML cap, respectively. For the 3 ML cap near the $\overline{\Gamma}$ point, the

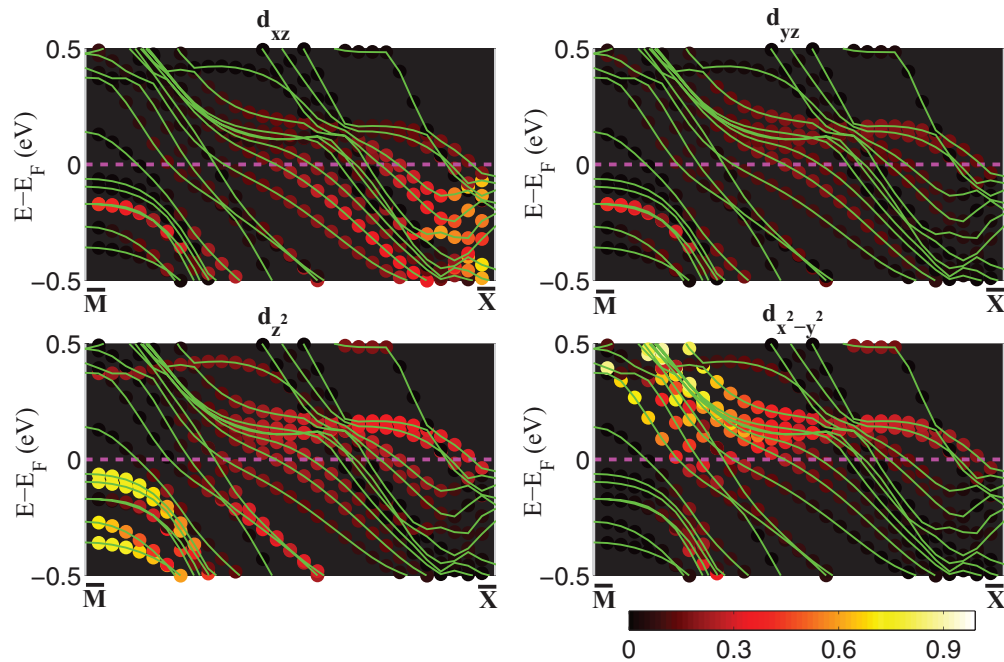


FIG. 12. (Color online) Energy- and k -resolved distribution of the Pd-cap-derived d_{xz} , d_{yz} , d_{z^2} , and $d_{x^2-y^2}$ orbitals along the \overline{MX} direction, with 3-ML-thick FePd films capped by 9 ML Pd.

unoccupied 1 and 2 bands in the top left panel are d_{xz} states, while the occupied 3 and 4 bands in the lower left panel are d_{yz} states. The SOC between these two states with the same m magnetic quantum number is coupled through the \hat{L}_z operator, which yields a positive contribution to the MCA(\mathbf{k}). In addition, the small energy separation between these states around E_F leads to the enhancement of the MCA for the 3 ML Pd cap. For the 4 ML cap, the additional Pd overlayer (upper and lower right panels) results in a new SPQWS (band 5), which in turn shifts up (down) the d_{xz} -band 1 (d_{yz} -band 3) from the Fermi energy leading in turn to a reduction of the MCA.

Upon increasing the Pd cap thickness, the number of bands increases and their d -orbital character along the various symmetry directions changes, resulting in corresponding changes of their contribution to the MCA. In particular, we find that the d_{xz} , d_{yz} , d_{z^2} , and $d_{x^2-y^2}$ orbital characters of the SPQWS are enhanced in the \overline{MX} region with increasing the cap thickness. Figure 12 shows the energy- and k -resolved distribution of these orbitals for the 9 ML cap. Note that the bands of d_{z^2} character extend both below and above the Fermi energy throughout most of the \overline{MX} direction, while those of $d_{x^2-y^2}$ are unoccupied. Furthermore, the bands of d_{xz} states are mainly occupied, while those of d_{yz} orbital character spread over both occupied and empty states. Consequently, the $\langle z^2 | \hat{L}_x | yz \rangle$ and $\langle x^2 - y^2 | \hat{L}_x | yz \rangle$ matrix elements which yield negative contributions to the k -resolved MCA lead to the monotonic decrease of the MCA with increasing cap thickness. Since the MCA $\rightarrow 0$ at about 8 to 10 cap ML, small changes in the electronic structure induced by additional capping layers induces the sign reversal of the MCA.

IV. CONCLUSION

In summary, we have carried out electronic structure calculations of the effect of the E-field and the heavy-metal cap of Pd on the magnetocrystalline anisotropy of FePd thin films. The underlying mechanism of the perpendicular MCA of the uncapped FePd film is the SOC between the unoccupied Fe d_{xy} and the occupied Fe $d_{x^2-y^2}$ states along the $\overline{\Gamma M}$ direction. In contrast, the SOC of the Pd occupied d_{z^2} states with the Fe unoccupied (d_{xz}, d_{yz}) states and the occupied Fe (d_{xz}, d_{yz}) states with the Pd unoccupied $d_{x^2-y^2}$ states gives a negative contribution to the MCA around the \overline{M} . The sensitivity of the surface MCA to the applied E-field of about 18 fJ/(V μ m) is due to the field-induced changes of the occupation of the surface Fe $d_{x^2-y^2}$ and (d_{xz}, d_{yz}) orbitals. We have demonstrated that the MCA changes dramatically by varying the Pd cap thickness, including a magnetization switching from an out-to in-plane orientation. The origin lies on the spin-polarized quantum well states induced by the cap, whose energies and orbital character depend on the cap thickness. These results have important implications on exploiting heavy metals with large SOC (Ru, Pd, Ta, Pt, or Au) as contacts with FM thin films to tailor the magnetic switching of spintronic devices by tuning the cap thickness.

ACKNOWLEDGMENTS

We thank Pavel Lukashev and Evgeny Tsymbal for helpful discussions. This research was supported by NSF Grant No. ERC-Translational Applications of Nanoscale Multiferroic Systems (TANMS)-1160504. Work in UCI was supported by DOES-BES (Grant No. DE-FG02-05ER 46237) and by NERSC for computing time.

-
- [1] D. C. Ralph and M. D. Stiles, *J. Magn. Magn. Mater.* **320**, 1190 (2008).
 - [2] E. Chen, D. Apalkov, Z. Diao, A. Driskill-Smith, D. Druist, D. Lottis, V. Nikitin, X. Tang, S. Watts, S. Wang, S. A. Wolf, A. W. Ghosh, J. W. Lu, S. J. Poon, M. Stan, W. H. Butler, S. Gupta, C. K. A. Mewes, T. Mewes, and P. B. Visscher, *IEEE Trans. Magn.* **46**, 1873 (2010).
 - [3] M. Weisheit, S. Fhler, A. Marty, Y. Souche, C. Poinsignon, and D. Givord, *Science* **315**, 349 (2007).
 - [4] K. Nakamura, R. Shimabukuro, Y. Fujiwara, T. Akiyama, T. Ito, and A. J. Freeman, *Phys. Rev. Lett.* **102**, 187201 (2009).
 - [5] C.-G. Duan, J. P. Velev, R. F. Sabirianov, Z. Zhu, J. Chu, S. S. Jaswal, and E. Y. Tsymbal, *Phys. Rev. Lett.* **101**, 137201 (2008).
 - [6] P. Ruiz-Díaz, T. R. Dasa, and V. S. Stepanyuk, *Phys. Rev. Lett.* **110**, 267203 (2013).
 - [7] M. Tsujikawa and T. Oda, *Phys. Rev. Lett.* **102**, 247203 (2009).
 - [8] T. Maruyama, Y. Shiota, T. Nozaki, K. Ohta, N. Toda, M. Mizuguchi, A. A. Tulapurkar, T. Shinjo, M. Shiraishi, S. Mizukami, Y. Ando, and Y. Suzuki, *Nat. Nanotechnol.* **4**, 158 (2009).
 - [9] M. K. Niranjan, C.-G. Duan, S. S. Jaswal, and E. Y. Tsymbal, *Appl. Phys. Lett.* **96**, 222504 (2010).
 - [10] M. Endo, S. Kanai, S. Ikeda, F. Matsukura, and H. Ohno, *Appl. Phys. Lett.* **96**, 212503 (2010).
 - [11] S. Ikeda, K. Miura, H. Yamamoto, K. Mizunuma, H. D. Gan, M. Endo, S. Kanai, J. Hayakawa, F. Matsukura, and H. Ohno, *Nat. Mater.* **9**, 721 (2010).
 - [12] Y. Shiota, T. Maruyama, T. Nozaki, T. Shinjyo, M. Shiraishi, and Y. Suzuki, *Appl. Phys. Express* **2**, 063001 (2009).
 - [13] D.-S. Wang, R. Wu, and A. J. Freeman, *Phys. Rev. B* **47**, 14932 (1993).
 - [14] S. Haraguchi, M. Tsujikawa, J. Gotou, and T. Oda, *J. Phys. D: Appl. Phys.* **44**, 064005 (2011).
 - [15] Y. Shiota, F. Bonell, S. Miwa, N. Mizuochi, T. Shinjo, and Y. Suzuki, *Appl. Phys. Lett.* **103**, 082410 (2013).
 - [16] C. Clavero, J. R. Skuza, Y. Choi, D. Haskel, J. M. Garca-Martn, A. Cebollada, and R. A. Lukaszew, *Appl. Phys. Lett.* **92**, 162502 (2008).
 - [17] F. Bonell, S. Murakami, Y. Shiota, T. Nozaki, T. Shinjo, and Y. Suzuki, *Appl. Phys. Lett.* **98**, 232510 (2011).
 - [18] P. E. Blöchl, *Phys. Rev. B* **50**, 17953 (1994).
 - [19] G. Kresse and J. Furthmuller, *Phys. Rev. B* **54**, 11169 (1996).
 - [20] G. Kresse and J. Furthmuller, *Comput. Mater. Sci.* **6**, 15 (1996).
 - [21] G. Kresse and J. Hafner, *Phys. Rev. B* **48**, 13115 (1993).
 - [22] J. Neugebauer and M. Scheffler, *Phys. Rev. B* **46**, 16067 (1992).
 - [23] D. D. Koelling and B. N. Harmon, *J. Phys. C: Solid State Phys.* **10**, 3107 (1977).

- [24] K. Nakamura, T. Akiyama, T. Ito, M. Weinert, and A. J. Freeman, *Phys. Rev. B* **81**, 220409(R) (2010).
- [25] L. Plucinski, Yuan Zhao, C. M. Schneider, B. Sinkovic, and E. Vescovo, *Phys. Rev. B* **80**, 184430 (2009).
- [26] R. Lorenz and J. Hafner, *Phys. Rev. B* **54**, 15937 (1996).
- [27] D. Weller, Y. Wu, J. Stöhr, M. G. Samant, B. D. Hermsmeier, and C. Chappert, *Phys. Rev. B* **49**, 12888 (1994).
- [28] R. Wu and A. J. Freeman, *J. Magn. Magn. Mater.* **200**, 498 (1999).
- [29] G. H. O. Daalderop, P. J. Kelly, and M. F. H. Schuurmans, *Phys. Rev. B* **41**, 11919 (1990).
- [30] D. Stoeffler, K. Ounadjela, J. Sticht, and F. Gautier, *Phys. Rev. B* **49**, 299 (1994).
- [31] U. Bauer, M. Dabrowski, M. Przybylski, and J. Kirschner, *Phys. Rev. B* **84**, 144433 (2011).
- [32] L. Szunyogh, B. Újfalussy, C. Blaas, U. Pustogowa, C. Sommers, and P. Weinberger, *Phys. Rev. B* **56**, 14036 (1997).
- [33] M. Cinal, *J. Phys.: Condens. Matter* **15**, 29 (2003).
- [34] M. Cinal and A. Umerski, *Phys. Rev. B* **73**, 184423 (2006).